Transactions of the **13th International Conference on Structural Mechanics in Reactor Technology** (SMiRT 13), Escola de Engenharia - Universidade Federal do Rio Grande do Sul, Porto Alegre, Brazil, August 13-18, 1995

Dynamic response of a containment surrounding extreme pressure source due to steam explosion

Yoshie, S.[1], Fukuda, H.[1], Maruyama, Y.[2], Yamano, N.[2], Sugimoto, J.[2]
1) Nuclear Systems Division, Kawasaki Heavy Industries Ltd., Tokyo, Japan
2) Japan Atomic Energy Research Institute, Ibaraki, Japan

1 INTRODUCTION

Based on the results of measurement of steam in a high-temperature high-pressure region (hereinafter referred to as a source) generated during steam explosion experiments, analytic models were developed, and such models showed possibility of reproducing those experiments. The energetic level of the source and structure of the containment vessel were subjected to parametric analyses with the help of the analytic models, and attention was paid to the mechanism of pressure wave propagation so as to understand the load applied to a containment vessel.

2 OUTLINE OF STEAM EXPLOSION EXPERIMENT IN ALPHA PROGRAM

In the event of a severe accident in a light water reactor (LWR), molten core component materials that contain fuels may contact with coolant during the core melt progression process. Pouring water over the molten core to positively cool it is considered as one of the accident management measures intended to mitigate the severe accident consequences. An interaction between the molten core and the water, which is referred to as a fuel/coolant interaction, may induce a steam explosion caused by the rapid transfer of energy stored in the molten core to the surrounding water in a very short period of time. The steam explosion that produces a great destructive force is possible to threaten the integrity of a reactor pressure vessel (RPV) or a reactor containment vessel (RPV) [1]. Under such circumstances, there have been many studies made to clarify the mechanism of the steam explosion and the load generated by the steam explosion [2].

In the Assessment of Loads and Performance of Containment in a Hypothetical Accident (ALPHA) program initiated at Japan Atomic Energy Research Institute (JAERI), melt drop steam explosion experiments (STX Experimental Series) are conducted [3] [4] [5]. The objectives of these experiments are to 1) understand the phenomena of steam explosion in a large-scale geometry and evaluate its characteristics, 2) clarify the load deposited to RPVs and RCVs by the steam explosion, 3) assess the influence of various

parameters that affect the occurrence and suppression of the steam explosion, 4) examine the effectiveness of conceivable accident management measures, and 5) obtain information necessary for development and verification of analytical models.

Figure 2.1 shows the conceptual diagram of the melt drop steam explosion experiments in the ALPHA program. The experiments were conducted in a model containment vessel. The major dimensions and capabilities of the model containment vessel are shown in Table 2.1. The thermite reaction of iron oxides (FeO and Fe_2O_3) with aluminum in the melt generator produced high-temperature melts consisting of iron and aluminum oxide (AL_2O_3), which were dropped into a steel or acrylic water pool placed in the model containment vessel. While the pressure, temperature, and level swell of the water in the pool were measured, the steam explosion was observed through a high-speed camera (approx. 4000 frames/s), as well as a high-speed video camera (500 frames/s). Since the steam explosion is an extremely rapid phenomenon, high-response piezoelectric pressure transducers were used, and their output was recorded by a 500 kHz high-speed data acquisition system.

So far, the melt drop steam explosion experiments were repeated 22 times, with the parameters of the mass of melts, ambient pressure of the model containment vessel, initial temperature and level of water, and the dispersing condition of melts in the water. The present analysis was made with respect to STX 019 in which the steam explosion was estimated to have been generated on the largest scale. Table 2.2 shows major experimental conditions of STX 019. In this experiment, an acrylic water pool shown in Fig. 2.2 was used, and a melt dispersion device was installed at a location 10 cm above the water surface. The melt dispersion device measuring 510 mm × 510 mm was shaped into a grid made of 3.2 mm dia. thin stainless steel wires with a pitch of 25 mm. Right before entering water pool, the melt was finely dispersed by the melt dispersion device. During the spontaneous steam explosion that occurred in STX 019, pressure peaks of approx. 20 MPa were observed in the water pool and those of approx. 0.4 MPa were observed in the atmosphere in the upper dome section of the model containment vessel.

3 METHOD OF ANALYSIS

3.1 *Analytic model*

AUTODYN-2D, V2.66+ was used as an analytic code. AUTODYN code [6] is physically formulated by continuum mechanics. The three phases of material (solid, liquid, and gas) can be dealt with in an integrated manner. Two types of formulation — Lagrangian and Eulerian methods — are known as the methods to describe continuums. In the current analysis, the water, source of steam explosion, air as atmosphere inside the containment vessel, were all expressed in Eulerian frame of reference, and the structural members were treated as a rigid boundary.

In Eulerian method, physical properties are expressed as functions of independent variables of x, y, z, and t. Physical property F of control volume having the coordinates (x, y, z) at time t will move to the coordinates (x + Δu, y + Δv, z + Δw) when a time Δt has passed. Therefore, the change in the physical quantity will be:

$$\Delta F = F(x + u\Delta t, y + v\Delta t, z + w\Delta t, t + \Delta t) - F(x, y, z, t)$$

$$= \frac{\partial F}{\partial x} u\Delta t + \frac{\partial F}{\partial y} v\Delta t + \frac{\partial F}{\partial z} w\Delta t + \frac{\partial F}{\partial t} \Delta t + O((\Delta t)^2)$$

When Δt approaches 0:

$$\frac{DF}{Dt} = u\frac{\partial F}{\partial x} + v\frac{\partial F}{\partial y} + w\frac{\partial F}{\partial z} + \frac{\partial F}{\partial t}$$

Of the terms in the formula, those up to the third one on the right side show the change accompanying the moving of material. In the meantime, the forth term shows the change with respect to the location of material when it is accelerated. In that case, the frame of reference is fixed in space, and material moves over it.

With respect to Eulerian method, the laws of conservation of mass, momentum, and energy are expressed by the following simultaneous partial differential equations of second order.

$$\frac{\partial \rho}{\partial t} + \frac{\partial}{\partial x_i}(\rho u_i) = 0$$

$$\frac{\partial u_i}{\partial t} + u_j \frac{\partial u_i}{\partial x_j} = f_i + \frac{1}{\rho}\frac{\partial \sigma_{ji}}{\partial x_j}$$

$$\frac{\partial e}{\partial t} + u_i \frac{\partial e}{\partial x_i} = f_i u_i + \frac{1}{\rho}\frac{\partial}{\partial x_j}(\sigma_{ij} u_i)$$

Where ρ is density, u_i is velocity, e is specific total energy, σ_{ij} is stress tensor, and f_i is external volume force per unit mass. The sum rule is used for suffix based on the ordinary tensor expression method.

In addition to the above three fundamental equations, an equation of state as a pressure estimation is simultaneously solved for both fluids and solids, and a constitutive equation as a deviatoric stress component estimation is solved simultaneously for solids.

In AUTODYN, the finite different method is adopted for discretization of hyperbolic partial differential equations of second order so as to solve them numerically. The analytic model used in the present analyses is shown in Fig. 3.1.

The model was symmetrical with respect to the axis of the two-dimensional cylinder. The appropriateness of advection calculation and integration errors, as well as the efficient calculation time, were checked by means of sensitivity analysis, and approx. 1000 meshes were provided for this parametric case study.

The walls and the base at the bottom of the containment vessel model were regarded as rigid boundaries. The pressure propagation as a load to the containment vessel, was paid attention and compared with the experiment.

For visualization, acrylic rectangular walls were used as water pool walls, which were destructed just after the steam explosion. It was understood, as the analysis progressed, that the initial existence of the water poll wall affected the expansion behavior of source as the high-temperature high-pressure gas after the steam explosion. Therefore the case where the water pool walls were regarded as rigid boundaries in the analytic model and the case where water pool walls were nonexistent from the beginning were compared with each other.

As shown in Fig. 3.1, the initial mesh of the source was made spherical as mush as possible in the analytic model so that it will properly reflect the volume of 0.08 m^3 which was assessed on the basis of the high-speed photographing result of the experiment (STX 005).

3.2 *Condition of analysis*

(1) Initial condition

When a phenomenon which triggers a steam explosion occurs in the region formed in a water pool where melt, water, and steam are coarsely mixed, a pressure wave generated there instantaneously propagates with fragmentation of the melt in the coarse mixing region. The melt fragmentation promotes increment of the area that is effective for heat transfer, and the thermal energy of the melt is rapidly transferred to the water. Therefore, in the coarse mixing region after propagation of the pressure wave, a high-pressure high-temperature state is created, and this region expands with the passage of time. Based on the observation with a high-speed camera in STX019, the pressure wave propagated through the coarse mixing region within 1 ms, and fragmentation of the melt was completed during this period. In addition, almost all of the melt that dropped into the water pool was fragmented into particles less than 2 mm, and the mass median particle diameter was approx. 200 μm. For the details of the experiment, refer to references [4] and [5].

It is necessary in the present analysis to set the location, volume, pressure, and temperature of the high-pressure high-temperature region formed in the water pool by the steam explosion as initial conditions. Based on the image, observed through a high-speed camera, of the coarse mixing region just before the steam explosion, the central position and volume of the high-temperature high-pressure region in STX019 were assessed at 0.2 m

below initial water level and 0.08 m^3, respectively. According to the volume of the coarse mixing region and the level swell of the water, the initial volumetric mixing ratios of the melt, water, and steam in the coarse mixing region were assessed at 0.063, 0.493, and 0.444, respectively. As an example of the coarse mixing region, the high-speed photo (STX005), which was taken just before steam explosion in the STX Experiment Series, is shown in Fig. 3.2. In this stage, the melt covered with a steam film was maintained at a high temperature, and the entire coarse mixing region was bright. After propagation of a pressure wave, the melt lost its heat rapidly and the region became dark, forming a high-pressure high-temperature region. Any significant difference in the volumes of the coarse mixing region and high-pressure high-temperature region just before and after propagation of the pressure wave was not observed.

The pressure and temperature of the high-pressure high-temperature region were found by thermodynamic calculations. For appraisal, the following assumptions were adopted: (1) steam in the high-pressure high-temperature region is an ideal gas, (2) the temperature of generated steam is elevated by restraint of its expansion (adiabatic compression), and (3) only the water that is vaporized reaches the saturation temperature, while the water remaining in the coarse mixing region maintains its initial temperature. Based on these assumptions, the equilibrium temperature inside the high-pressure high-temperature region and the mass of vaporized water were calculated with the following equations:

$$xM_mC_{pm}(T_m - T_e) = M_v(C_{pw}\Delta T_{sub} + \Delta H_{lv}) \qquad (1)$$

$$v_v(M_{vi} + M_v)T_v^{Cvv/R} = (V_{vi} + v_wM_v)T_e^{Cvv/R} \qquad (2)$$

Where
- C_{pm} : Specific heat of melt
- C_{pw} : Specific heat of water at constant pressure
- C_{vv} : Specific heat of steam at constant volume
- M_m : Total mass of melt
- M_v : Mass of vaporized water (mass of generated steam)
- M_{vl} : Mass of initial steam in coarse mixing region
- R : Gas constant
- T_e : Equilibrium temperature inside high-pressure high-temperature region
- T_m : Initial temperature of melt
- T_v : Saturated steam temperature under atmospheric pressure
- ΔT_{sub} : Subcooling of water
- ΔH_{lv} : Latent heat of vaporization of water
- V_{vi} : Initial volume of steam in rough mixing region
- v_v : Specific volume of steam
- v_w : Specific volume of water
- x : Mass ratio of melt that participates in steam explosion

The equilibrium pressure in the high-pressure high-temperature region will be obtained by substituting the equilibrium temperature and the mass of vaporized water found by the above two equations into the equation of gas state. Supposing the all melt participates in the steam explosion, the equilibrium pressure, equilibrium temperature, and mass of vaporized water are approx. 83 MPa, 1347 K, and 10.4 kg, respectively. When 30% of the melt concerns steam explosion, they will be approx. 24 MPa, 1058 K, and 3.7 kg, respectively.

(2) Analyzed cases

Table 3.1 shows a list of cases analyzed, as well as the values of physical properties. Parameters were used to represent the pressure and temperature of the source, presence/absence of water pool walls, and upper dome shape of the containment vessel, and four cases in total were analyzed. The initial position of the center of the source and its initial volume, as well as the quantity of saturated water in the water pool, were all regarded as invariable.

Case A : Where the total volume of the melt was assumed to have related to the steam explosion, and the source showed the higher pressure (83 MPa). Water pool walls (rigid) existed in this case.

Case B : Where 30% of the melt was assumed to have related to the steam explosion in the same system as Case A, and the initial pressure was 24 MPa. The experimental results were expected to stay somewhere between Case A and Case B.

Case C : In comparison with Case B, water pool walls were nonexistent. Comparison between Case B and Case C permits analysis of the effect of water pool walls.

Case D : In comparison with Case C, the upper dome of the containment vessel model was made to be flat to clearly show the features of the propagation behavior of the pressure waves when the dome was semi-elliptical.

4 ANALYSIS OF RESULTS AND DISCUSSION

Figure 4.1 shows the output points (hereinafter referred to as target points) of the analytical results.

(1) Expansion behavior of source and pressure wave propagation

Figure 4.2 shows the comparison of plotted velocity vectors and the source boundary between Case A and Case B. In Case A, the vectors in the axial direction exceed that in the radial direction because of the higher pressure level of the source and the presence of the

water pool boundary, and pressure waves reach the top of the containment vessel in the axial direction earlier than the side in the radial direction. In Case B, vectors in the axial and radial directions are equal, and pressure waves reach the flank of the containment vessel earlier, since the distance to the flank is shorter than to the top (h/d).

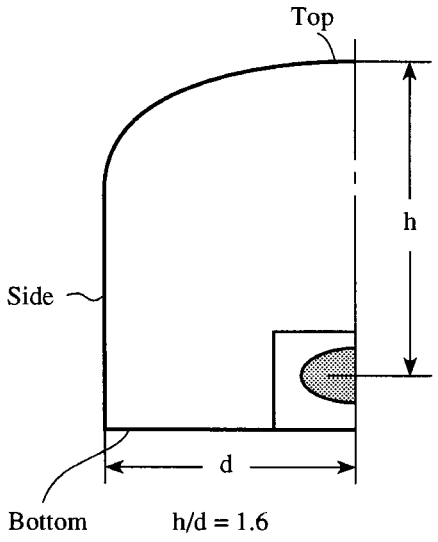

Figure 4.3 shows pressure history with a peak value of 60 MPa and duration of 1.5 ms at a location (target 27) just above the source in Case A. The peak value attenuated as a spherical wave to 7 bars (target 32) and was reflected from the top, increasing to 14 bars. Figure 4.4 shows the comparison of pressure history at target 1 between Case A and Case B.

The pressure wave propagation speed in the axial direction in Case B was 780 m/s, while that in Case A was faster. Of the pressure waves in Case B shown in Fig. 4.4, the second wave (indicated by an arrow in the figure) appeared because, as stated before, the pressure wave that once reached the side of the containment vessel was reflected to concentrate in the center of the containment vessel and began to propagate again in upward the axial direction. (See the portion "a" in Fig. 4.5.)

(2) Comparison between experiment and analysis

In the experiment, pressure was measured at target 4, which is shown in Fig. 4.6 together with the pressure history in Case A and Case B of the analysis. Case A shows the pressure rising slope and peak pressure value that are close to the experiment results. The experimental results stayed between Case A and Case C.

In short, it is suggested that the contribution rate of the melt to the steam explosion was estimated between 30% and 100%.

In the experiment, the axis symmetry of the steam explosion phenomenon, as well as the simultaneity of reflection of pressure waves from the flank of the containment vessel, cannot be maintained; therefore, the second pressure wave (indicated by an arrow in Fig. 4.6) is not considered to be clear.

In the future experiments, the number of pressure measurement points in the containment vessel model is planned to be increased so as to permit more detailed comparison with analysis.

(3) Effects of water pool wall and shape of containment vessel dome

In cases where there is no pool wall from the beginning, the water in the pool has the freedom to move in the radial direction when the source pressure is applied, and the expansion behavior of the source is different from the case where there are pool wall. Figure 4.7 shows vector plots comparing the case with/without pool wall. As shown in the right half of the same figure, the source presses down and expands radially the water in the absence of pool wall.

As a result, the propagation speed of pressure waves in the axial direction reaching the top drops to 540 m/s, and the pressure level drops at the same time.

Figure 4.8 shows the pressure history at target 1, comparing between Case B (with pool wall) and Case C (without pool wall). As indicated by the arrow in the figure, higher peak pressure appears later than 10 ms when there is no wall. It is considered that pressure waves reflected from the side of the containment vessel and the basement propagate along the shape of the upper dome of the containment vessel and concentrate at the top, thereby increasing the pressure. Unlike Case C, the flat roof of the containment vessel (Case D) did not allow the pressure to increase prominently.

5 CONCLUSIONS

In the present analysis, the steam (source) in the high-temperature high-pressure region caused by the steam explosion was dealt with as an ideal gas initialized with the help of experimental results, and attention was paid to the behavior of the pressure wave propagation inside the containment vessel model. In the analysis, parameters were used to represent the source pressure, presence/absence of water pool walls, and the shape of containment vessel. The findings are summarized below.

(1) After the possibility of analysis to explain the experiment results was found, the rate of contribution of melts to the steam explosion in the current experiment was predicted.

(2) When water pool walls are regarded as rigid in the analytic model, the pressure is expressed as a vector in the axial direction, and a higher pressure is generated at the top of the containment vessel. At the same time, after first pressure wave has reached, another pressure wave reflected from the flank appears later. Such behavior depends on the ratio "h/d" of respective containment vessels configuration.

(3) When there is no water pool walls, the water in the pool moves in the downward and radial directions by the source pressure, and the propagating pressure inside the containment vessel is comparatively small. It was found, however, that pressure waves concentrate at the top after propagating along the semi-elliptical shape of the top of the containment vessel, and the peak pressure higher than that observed in the

presence of water pool walls is generated. Therefore, in terms of the load condition applied to the containment vessel under steam explosion, assessment should be made according to the respective structures of containment vessels.

REFERENCES

[1] T. G. Theofanous, B. Najafi and E. Rumble, An assessment of steam explosion induced containment failure, Part I: probabilistic aspects, Nucl. Sci. Eng. 97 (1987) 259-281.

[2] M. L. Corradini, B. J. Kim and M. D. Oh, Vapor explosions in light water reactors: A review of theory and modeling, Progress in Nuclear Energy 22 (1988) 1-117.

[3] NURETH-5.

[4] CSNI Specialist Meeting, to appear.

[5] Nucl. Eng. and Des., to appear.

[6] N. K. Birnbaum, M. S. Cowler, M. Itoh, M. Katayama, H. Obata, AUTODYN - an interactive dynamic analysis program for microcomputers through supercomputers, 9th SMiRT, August 1987, Lausanne, Switzerland.

ACKNOWLEDGMENT

The authors wish to express their thanks to Mr. M. Katayama of CRC for his technical advice with respect to the AUTODYN code.

Table 2.1 Remarks of ALPHA Containment Model

Volume	50	m^3
Height	5.7	m
Diameter	3.9	m
Design pressure	2	MPa
Design temp.	523	K

Table 2.2 Experimental Conditions (STX019)

Ambient pressure	0.1	MPa
Atmosphere	Air	
Melt composition	Iron/Alumina thermite	
Melt mass	20	kg
Melt temp.	~ 2700	K
Melt falling distance	3.5	m
Initial water temp.	281	K
Initial water depth	0.9	m

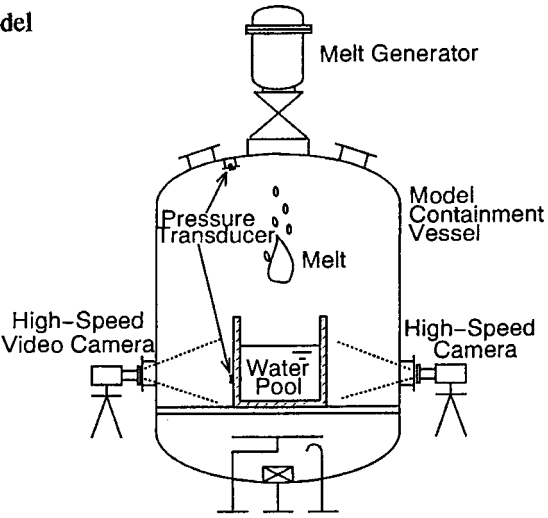

Fig. 2.1 Conceptual diagram of melt drop steam explosion experiments

Table 3.1 Parametric List of Analytical Cases

			Case A	Case B	Case C	Case D
Analytical Model			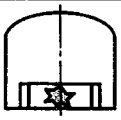	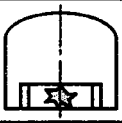	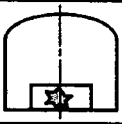	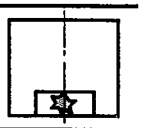
Upper Shape of Containment			Spherical	Spherical	Spherical	Plane
Water Pool(Rigid Boundary)			Exist	Exist	No	No
Source	Initial Pressure	[MPa]	83	24	24	24
	Initial Volume	[m^3]	0.08	0.08	0.08	0.08
	Initial Temperature	[K]	1347	1058	1058	1058
	Specific Heat(Cv)	[kJ/kgK]	2.89	3.86	3.86	3.86
	Specific Heat Ratio	[/]	1.77	1.32	1.32	1.32
	Reference Density	[g/cm^3]	8.03×10^{-4}	8.03×10^{-4}	8.03×10^{-4}	8.03×10^{-4}
Water	Initial Pressure	[MPa]	0.1	0.1	0.1	0.1
	Initial Volume	[m^3]	0.33	0.33	0.33	0.33
	Initial Temperature	[K]	281	281	281	281
	Specific Heat(Cv)	[kJ/kgK]	4.5(at 393K)	4.5(at 393K)	4.5(at 393K)	4.5(at 393K)
	Reference Density	[g/cm^3]	1	1	1	1
Air	Initial Pressure	[MPa]	0.1	0.1	0.1	0.1
	Initial Volume	[m^3]	41.2	41.2	41.4	41.4
	Initial Temperature	[K]	281	281	281	281
	Specific Heat(Cv)	[kJ/kgK]	0.725(at 373K)	0.725(at 373K)	0.725(at 373K)	0.725(at 373K)
	Specific Heat Ratio	[/]	1.396	1.396	1.396	1.396
	Reference Density	[g/cm^3]	1.225×10^{-3}	1.225×10^{-3}	1.225×10^{-3}	1.225×10^{-3}

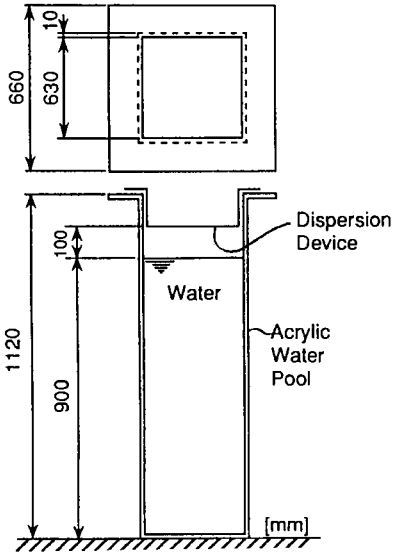

Fig 2.2 Water Pool

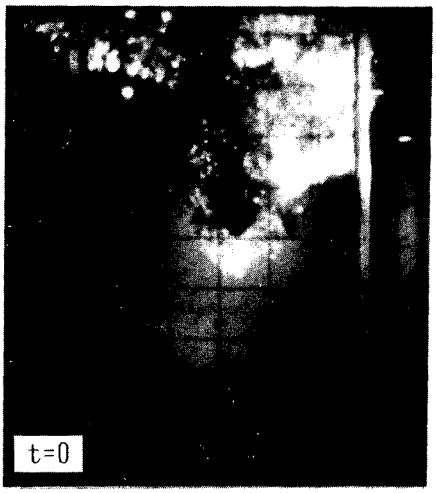

Fig. 3.2 High-speed Photo Just before Steam Explosion

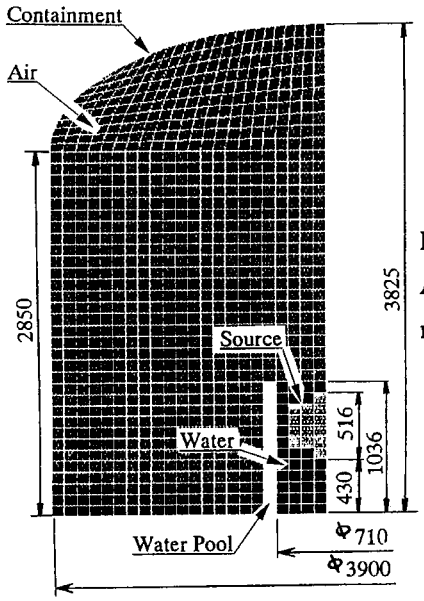

Fig.3.1 Analytical model

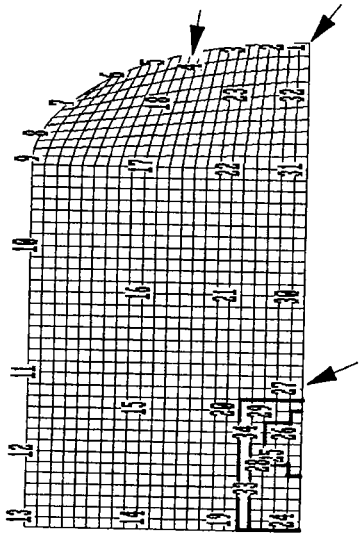

Fig.4.1 Target Points

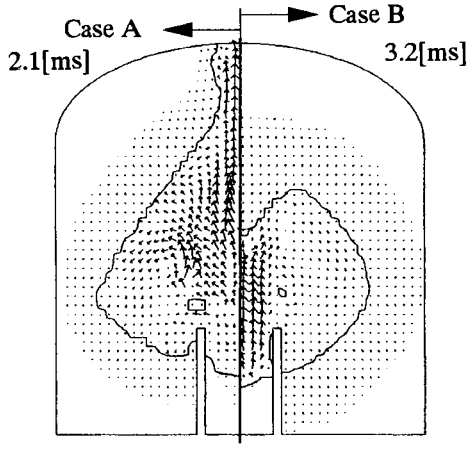

Fig.4.2 Vector Plot

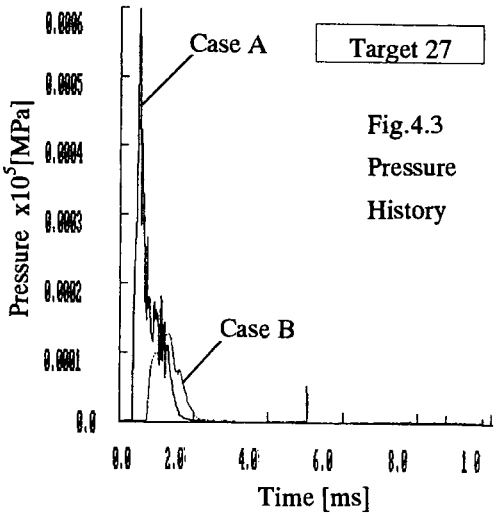

Fig.4.3 Pressure History

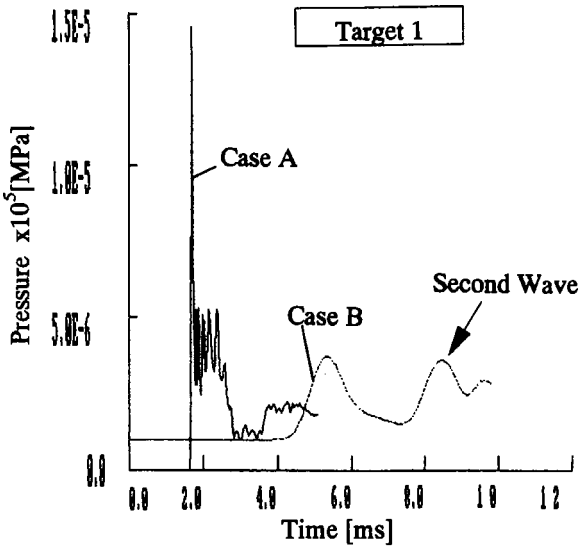

Fig.4.4 Pressure History

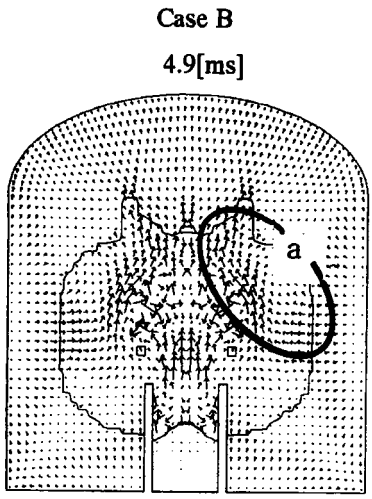

Fig.4.5 Vector Plot

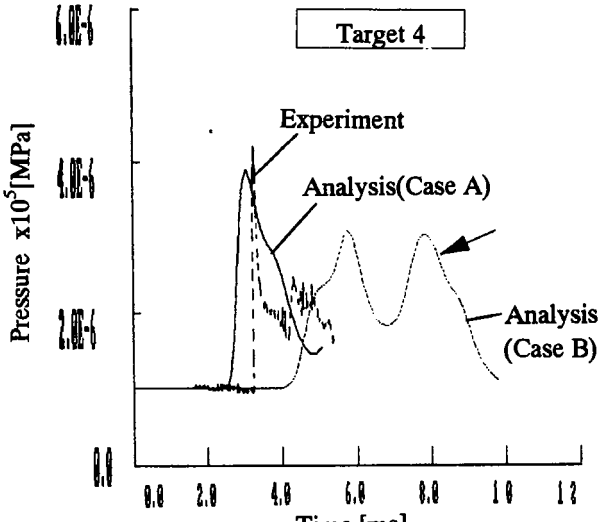

Fig.4.6 Pressure History

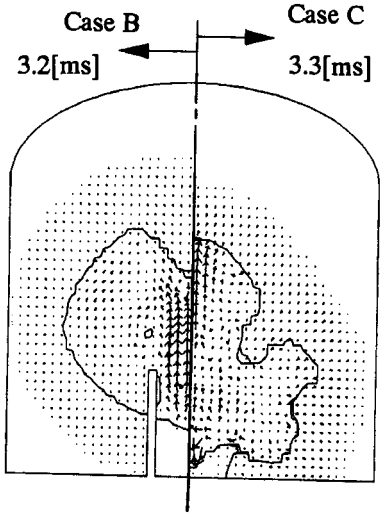

Fig.4.7 Vector Plot

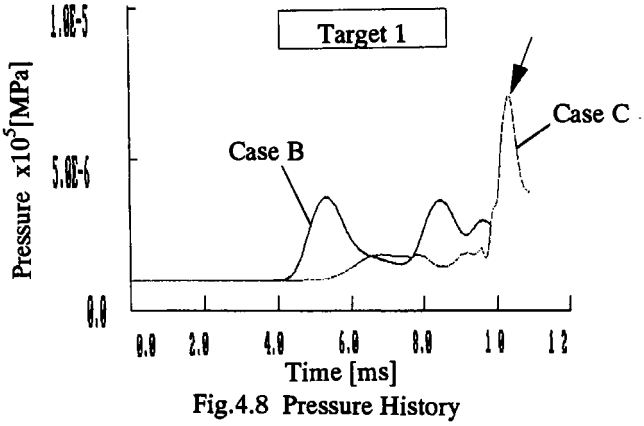

Fig.4.8 Pressure History